The Effect of Shear Deformation on Nylon-6 and Two Types of Nylon-6/Clay Nanocomposite

Jisheng Ma, George P. Simon, and Graham H. Edward*

Department of Materials Engineering, Monash University, Melbourne, VIC 3800, Australia

Received July 16, 2007; Revised Manuscript Received October 10, 2007

ABSTRACT: The crystalline orientation in nylon-6 and the crystalline and clay layer orientation in nylon-6/clay nanocomposites produced by 90° equal channel angular extrusion (ECAE) are reported. A temperature of ca. 150 °C was necessary to obtain the highest permanent shear strain for both nylon-6 and nylon-6/clay nanocomposites, the nanocomposites produced by either melt blending or in situ polymerization. Nylon-6 was found to affinely deform, while the introduction of the clay causes a nonaffine deformation of the crystal ellipsoids. By comparison of the orientation angle of clay layers from small angle X-ray scattering, the orientation angle of crystal ellipsoids from polarized optical microscopy, the calculated orientation angle from the apparent shear strain, and the main orientation direction of macromolecular chains, the mechanism of clay layer slip was proposed to explain the results of the high orientation of the macromolecular chains and the lagged orientation of the crystal ellipsoids in nylon-6/clay nanocomposite during ECAE process. The in situ polymerized nylon-6/clay nanocomposites achieved the highest orientation, which can be explained by the covalent connection of molecular chains and clay layers in this system.

Introduction

It is widely known that molecular orientation in polymers can be utilized for improving the physical and mechanical properties.[1−3] Numerous research efforts have focused on controlling molecular anisotropy in the fabrication processes used to produce fiber and film. Unlike processes in melt or solution, equal channel angular extrusion (ECAE) is a solid-state process, with the polymer being deformed well below its normal processing or melt temperature. The process is seen as a potential alternative to other solid-state processes such as hydrostatic extrusion, die drawing, and cold drawing that have been extensively investigated in the past[1,4] with a view to fabricating monolithic polymer parts with controlled anisotropy.

The success of the ECAE process in modifying metal properties has led to research to determine whether it is a feasible means of controlling molecular orientation and microstructural anisotropy in polymers.[2−7] In principle, the ECAE process can impose a uniform simple shear deformation on an extrudate without altering its cross-sectional dimensions. Since the polymer is extruded in the solid state, significant molecular orientation takes place as a result of such a high degree of plastic deformation by simple shear. This solid-state extrusion process is potentially more effective in generating a high degree of molecular orientation than processes involving extrusion in the molten state. The current ECAE setup has the potential to be modified into a more cost-effective continuous extrusion process by attaching an ECAE die to a conventional extrusion unit.[3]

The ECAE process has been used recently to produce deformation in polyethylene, polypropylene,[1] polycarbonate,[5−6] and poly(ethylene terephthalate).[2,7] Nylon-6/clay nanocomposites were the first successful nanocomposite system reported, demonstrating a dramatic improvement in properties,[8] usually on samples produced by injection molding. Many aspects of the mechanism of reinforcement have been widely reported, including the conformation and morphology of polymer chains[9] and the crystalline structure transformation influenced by the introduction of a small amount of clay.[10−11] Sue et al.[12−13] reported recently the effect of ECAE processing on the morphology and mechanical properties of nylon-6 and nylon-6/clay nanocomposites. The current work reported here considers in more detail the effect of clay on the deformation behavior and orientation in the crystalline region as well as the orientation of the clay layers themselves. Particularly, the mechanisms of clay-induced crystal lamellae and molecular chain orientation are discussed. The orientation of α-form crystals in nylon-6 is investigated in order to determine the impact of the clay on the crystalline orientation occurring during ECAE process. The orientation of the macromolecular chains was studied, and the mechanism of orientation is discussed.

Experimental Section

Two pairs of nylon-6 and nylon-6/clay materials were used in the investigations, these pairs being chosen so that the homopolymer nylon in each case is similar to the matrix nylon in the corresponding nanocomposite. One pair of materials was supplied by RTP company (US) and the other by Honeywell company (US). These materials were RTP 200A (nylon-6 alone, obtained from the RTP company, abbreviated herein as R), RTP 299A X83133C (nylon-6/clay nanocomposite, from RTP company, with the clay incorporated by melt blending and abbreviated herein as RN), Capron 8202 NL (nylon-6 alone, from Honeywell, abbreviated herein as C), and Capron XA2908 (nylon-6/clay nanocomposite, from Honeywell, with the clay incorporated by in-situ polymerization and abbreviated herein as CN).

The RN and CN contain 3.5 ± 0.5 and 2.9 ± 0.2 wt % nanoclay, respectively, according to TGA measurements under argon gas flow on these materials.[14] The samples were obtained in pellet form and were dried under vacuum at 100 °C for 14 h prior to compression molding into 10 mm thick, 150 mm side square samples. The hydraulic press and the metal plates used for compression molding were preheated to 265 °C and, after adding the granules, the plate assembly was kept at 265 °C for 5 min before pressure was applied. The pressure was kept constant as the mold was gradually cooled to 240 °C over approximately 15 min. The compression molding was then allowed to naturally cool to room temperature under pressure, which took 3 h in total.

* To whom correspondence should be addressed. E-mail: graham.edward@eng.monash.edu.au.

10.1021/ma071580o CCC: $40.75
Published on Web 12/15/2007

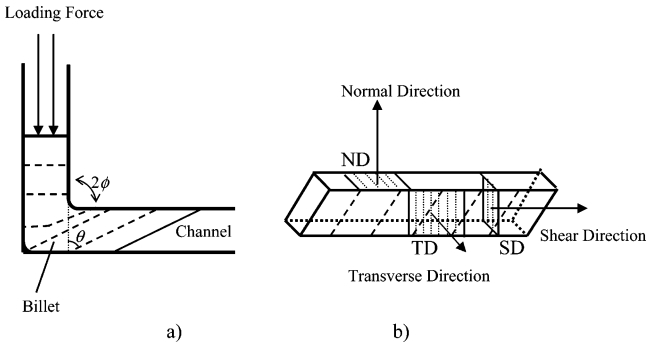

Figure 1. (a) Schematic diagram of the equal channel angular extrusion (ECAE) process. (b) Normal directions of the three slices cut for X-ray investigation from the billets.

The 10 mm thick sheets were cut into 18 mm wide × 80 mm long billets for the ECAE process. The billets after the ECAE process were further sliced into 1 mm thick samples using an ACCUTOM-20 (Struers) cutting machine for X-ray investigations. Undeformed billets were also cut into the same size samples for comparison.

A schematic of the ECAE process is shown in Figure 1a. The rig is a steel block with two intersecting channels of identical cross section. A billet of material is pushed along one of the channels and around the bend into the second channel. Ideally, the specimen undergoes simple shear uniformly across a thin layer located around the plane where the two channels intersect. The entire billet can thus be deformed homogeneously by this method except for the end regions. ECAE is unique in that it imposes a uniform, through-thickness simple shear deformation on the extrudate without altering the dimensions of extrudates[6] due to the constant displacement across the channel caused by the rigid push rod. This is in contrast to the pressure driven melt flow found in processes such as injection molding, where deformation gradients are found from the surface to the interior of the material. In principle, the process could be repeated indefinitely, increasing the shear with each pass. Alternatively, the shear could be cancelled by reversing the billet for the second pass.

The plastic shear strain increment γ that occurs in N passes with no billet reversal depends on the angle 2φ between the intersecting channels and is given by

$$\gamma = 2N \cot \varphi \quad (1)$$

This simple relationship assumes complete and homogeneous plastic deformation in the extrusion process and ignores any strain gradients, elastic bending, and possible viscoelastic effects that may occur. The value of γ given by eq 1 is an upper limit to the plastic strain achievable in N passes,[1] and for example, with one pass through a right angle corner, where 2φ is 90°, γ is equal to 2.

X-ray diffraction specimens were taken from the central portions of the billets and cut into 1 mm thick planar slices, and the normal of the specimen was aligned with the direction of the radiation, this being with respect to the transverse direction, normal direction, or shear direction, as shown in Figure 1b. The resultant X-ray transmission diffractograms were designated as TD, ND, and SD, respectively.

Additional experiments called channel die compression (CDC) were performed using a channel die illustrated in Figure 2, which was used to apply pure shear to samples. The three directions related to the billet in the shearing process are designated as the compression direction (CD), the transverse direction (TD), and the flow direction (FD). The plane strain flow is such that the strain along TD is zero.

X-ray transmission diffraction flat plate films were obtained with a Philips X-ray machine. Cu Kα radiation of 0.154 nm in wavelength (λ) generated at 40 kV and 20 mA was used for the diffractograms, which were taken by transmitting a 1 mm diameter X-ray beam through the 1 mm thick sample. A piece of film was placed behind the sample thus capturing the diffraction pattern. The distance between the film and the specimen was 30 mm. X-ray diffraction scans of the specimens were obtained with a Rigaku-Geigerflex (Japan) wide angle X-ray diffractometer (WAXD) using Ni filtered Cu Kα radiation at a generator voltage of 40 kV and a current of 30 mA, utilizing transmission mode. The scanning rate was 2 deg/min, and the diffracted intensity was recorded automatically at intervals of 0.02°.

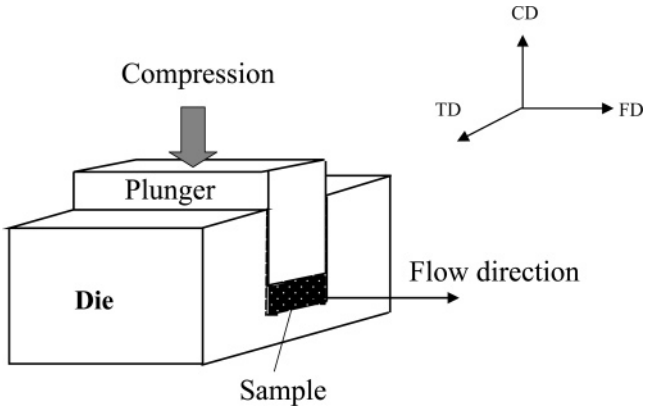

Figure 2. Schematic diagram of the channel die compression (CDC) process.

Transmission polarized optical microscope photographs were obtained by using a Japan Olympus BH-2 polarizing microscope. The samples were microtomed into 20 μm slices and sandwiched between microscope cover slips.

Additional X-ray scattering experiments were performed at room temperature using the synchrotron beamline of the Australian National Beamline Facility (ANBF) at the Photon Factory in Tsukuba, Japan. The ANBF beamline is installed on a bending magnet port and delivers monochromatic synchrotron X-rays in the energy range 4.5−20 keV to the experimental station in a hutch. The resolution of the diffractometer mode is 0.0005° in 2θ. The instrument has a multiconfiguration vacuum diffractometer that uses image plates as its detector system. Small angle X-ray scattering (SAXS) was performed by setting the wavelength at 0.2 nm with a beam size of 200 μm × 200 μm. The specimens were mounted at the center of the ANBF vacuum diffractometer at a distance of 570 mm from the image plate. Two-dimensional SAXS patterns were obtained with the X-ray beam passing through the transverse direction of deformed samples. The X-ray scattered intensity recorded on the image plate was extracted from the raw image data and then converted to a recognizable format, e.g., scattered intensity I versus angle 2θ, using PPDA software. Scattering without the specimen was recorded as a background scattering I_b, to enable correction of measured SAXS patterns.

Results and Discussion

Figure 3 shows the effect of temperature on the shear strain achieved by nylon R after the ECAE process. At low temperatures (<135 °C), the R billet does not attain a high shear strain. When the ECAE temperature is increased, the permanent shear strain of the extruded R billet increases until the temperature reaches about 145 °C. Further increasing of the ECAE temperature has little subsequent effect on the shear strain. The reason for this temperature dependence may be attributed to the increasing mobility of macromolecular chains with increasing temperature and the need to be sufficiently above the glass transition temperature of the nylon-6 (T_g = 56 °C) to permit appreciable plastic deformation. With increasing temperature, the molecular chains become sufficiently flexible so that most chains in the amorphous regions can be moved by the shear force, permitting deformation of the spherulites and more plastic strain being acquired by the billet. It can be concluded from Figure 3 that the optimum ECAE temperature to obtain relatively

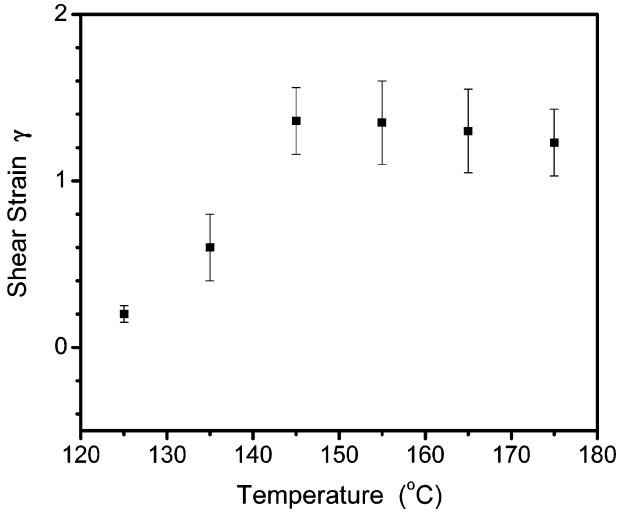

Figure 3. The effect of extrusion temperature on the permanent shear strain of nylon-6 after the first ECAE process.

high shear deformation is about 150 °C. Further increase in the temperature is likely to decrease the amount of molecular orientation obtained despite the plastic strain being roughly constant with increasing temperature. A similar situation has been found when orienting polyethylene by tensile drawing, where although the attainable plastic tensile strains increase with increasing temperature, the extent of orientation decreases as the melting temperature is approached, and an intermediate temperature is best for obtaining molecular orientation.[4] Subsequently, the ECAE process was carried out at 150 °C and an extrusion rate of 10 mm/min was used for most of the results reported fromhere.

Figure 4 shows views of the billets after the CDC and the ECAE processes. The original square grid lines of the billet after the ECAE process are deformed and tilted at an angle θ away from the normal direction (see Figure 2). The plastic shear strain γ induced by the ECAE process was calculated from the shear angle θ by $\gamma = \tan(\theta)$. The CDC deformation is clearly nonhomogeneous (due to friction with the die), but samples were taken from the central portion of the specimens, where the deformation is relatively homogeneous as judged from the grid patterns. Strains due to CDC were estimated from the spacing of the horizontal grid markings.

Figure 5 shows typical loading stress vs plunger displacement curves obtained during the ECAE process. In the early stage of the extrusion, as the material conforms to the die channel corner, the load increases as more material yields across the width of the extrudate. Once the leading end of the billet is completely around the corner, it is expected that the load is constant, as an unchanging volume of material will be undergoing yield, and the process has achieved steady state. Figure 5a shows that the plunger load for nylon-6 is almost constant after the deformation becomes established. The maximum stress for the nylon-6/clay nanocomposite is higher than that for the nylon-6 but decreases noticeably during the ECAE process and finally becomes lower than nylon-6 samples. The reason may lie in the fact that the temperature increase of samples during the ECAE process that has been observed for poly(ethylene terephthalate)[2] may be occurring here, leading to a change in the yield stress, a change in the deformation zone geometry, or a change in the frictional resistance to continuing extrusion. The maximum stress for nylon-6/clay nanocomposites in a second ECAE pass is found to be lower than that in first pass (in Table 1), but the stress does not decrease as fast as for the first pass (see Figure 5b).

Multiple samples of both the nylon-6 and the nylon-6/clay nanocomposites were processed by ECAE (simple shear) and CDC (pure shear) at a temperature of 150 °C. Although there was some small variation between ostensibly identical samples, the average values of the maximum stress and strain from three to five repeated tests and their standard deviations were obtained. The roughly constant ram stress for ECAE and the resultant shear strain of the deformed materials are listed in Table 1 along with corresponding data from the CDC tests. The maximum stress for the channel die deformation is the load divided by the compressed area. It can be seen that shear strains around 1.3−1.5 were obtained for the four different materials when subjected to ECAE compared with the theoretical value of 2.0. This discrepancy is due to nonideal deformation in the die, with the elements of bending and elastic deformation replacing the plastic deformation. The channel die deformations were stopped at a similar strain level to allow for later comparison between the microstructures. It can be concluded that both the CDC and the ECAE process can apply significant apparent plastic shear strain to the different materials.

The first pass of ECAE applied a similar shear strain to all four materials. Compared to the loading stress and the shear strain in the first pass, it can be seen that in the second pass for nylon-6 R a similar loading stress was needed and an increased shear strain was obtained but for the nylon-6 C a lower loading stress was required but the shear strain was not enhanced. However, for nylon-6/clay nanocomposites, the result is quite different; in both cases increased shear strain can be obtained but with less stress in the second pass than in the first pass. In addition, for CN with the lowest stress during the second pass, the highest shear strain was obtained. A possible explanation is that the orientation of the clay layers distributed in the polymer matrix has a positive effect on promoting plastic deformation. Details will be discussed later.

In order to characterize the orientation produced by the shear strains and to compare the shear-induced orientations obtained by the CDC and ECAE process, a WAXD scan along the azimuthal direction where the α (002) is maximum with the transmitted beam along TD for the samples C and CN was carried out and the results are shown in Figure 6. The clay-induced chain orientation in nylon-6/clay nanocomposites is complex because of the coexistence of the α and γ crystalline forms. It is well-known that the addition of nanoclay to nylon-6 results in an enhancement of the γ crystalline phase, which is also observed by spinning fibers at a high speed in rapidly cooled nylon-6 homopolymer or by iodine treatment of nylon-6 in aqueous KI/I_2 followed by removal of the iodine and potassium with sodium thiosulfate.[15] If the content of γ crystals is relatively large, the orientation and deformation of the crystalline components are governed more by the behavior of

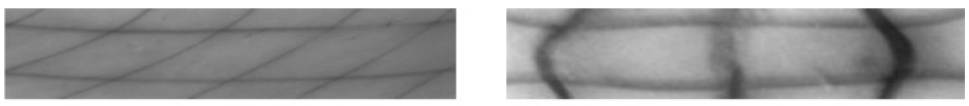

Figure 4. Side view of grid line changes after (a) ECAE at 150 °C and (b) CDC at 150 °C.

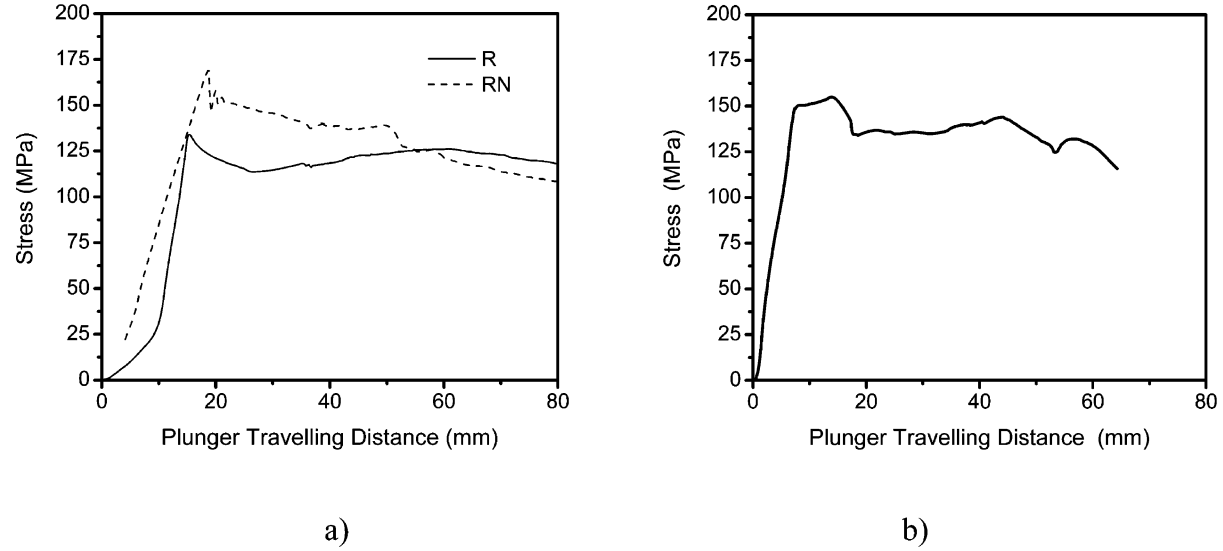

Figure 5. Typical curves of loading stress vs plunger traveling distance during the ECAE process at 150 °C: (a) first pass of R and RN; (b) second pass of RN.

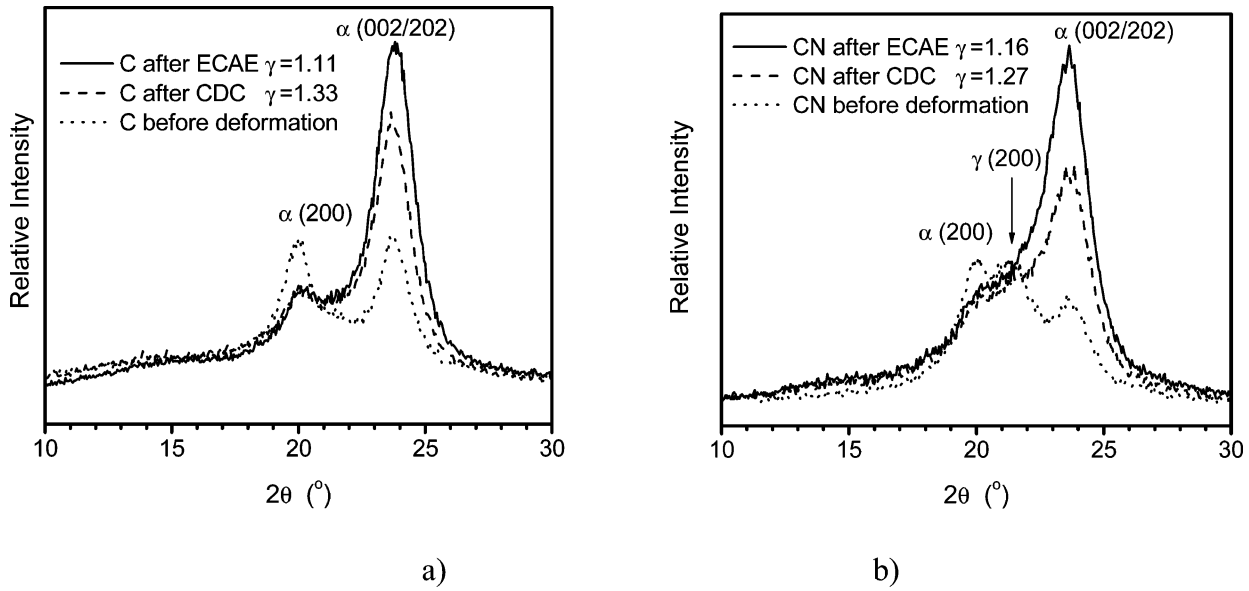

Figure 6. The WAXD scans along the α (002) high diffraction direction of the undeformed material and after the CDC and the ECAE processes for (a) C and (b) CN.

Table 1. A Comparison of ECAE and CDC Deformations

	ECAE				CDC	
	first pass		second pass			
	stress (MPa)	shear strain	stress (MPa)	shear strain	stress (MPa)	shear strain
C	127 ± 9	1.4 ± 0.2	115 ± 8	1.4 ± 0.1	110 ± 5	1.3 ± 0.1
CN	154 ± 9	1.5 ± 0.2	110 ± 8	2.0 ± 0.3	110 ± 5	1.4 ± 0.1
R	135 ± 9	1.5 ± 0.2	135 ± 2	1.8 ± 0.1	100 ± 5	1.3 ± 0.1
RN	167 ± 9	1.3 ± 0.2	153 ± 2	1.6 ± 0.1	100 ± 5	1.4 ± 0.1

γ crystals, the orientation and deformation of the remaining α crystals also being governed by the deformation of γ crystals.[16] Alternatively, in the situation as in CN (see Figure 6 b) where the α phase still predominates, the orientation and deformation of the crystalline components will be governed by the behavior of α crystals.[16] Therefore, the diffraction from α crystals is used to quantify the orientation produced by deformation in both cases.

When the α (200) diffraction is set at the same intensity, the relative intensity from α (002) of C and CN after the ECAE process is higher than that of the two samples after CDC even though the strains (γ = 1.11 and 1.16, respectively) by the ECAE process are smaller than those (γ = 1.33 and 1.27, respectively) produced by CDC. It is evident that the higher apparent shear strains do not necessarily ensure that higher orientations are produced and that the deformation path or stress state may play a role. This also indicates that the ECAE process seems to produce higher orientation than does the CDC for similar strain levels. Also, shown in Figure 6 is the diffractometer trace for the undeformed material in each case and it is evident that the deformation induces an orientation that enhances the α (002) diffraction while diminishing the α (200) diffraction

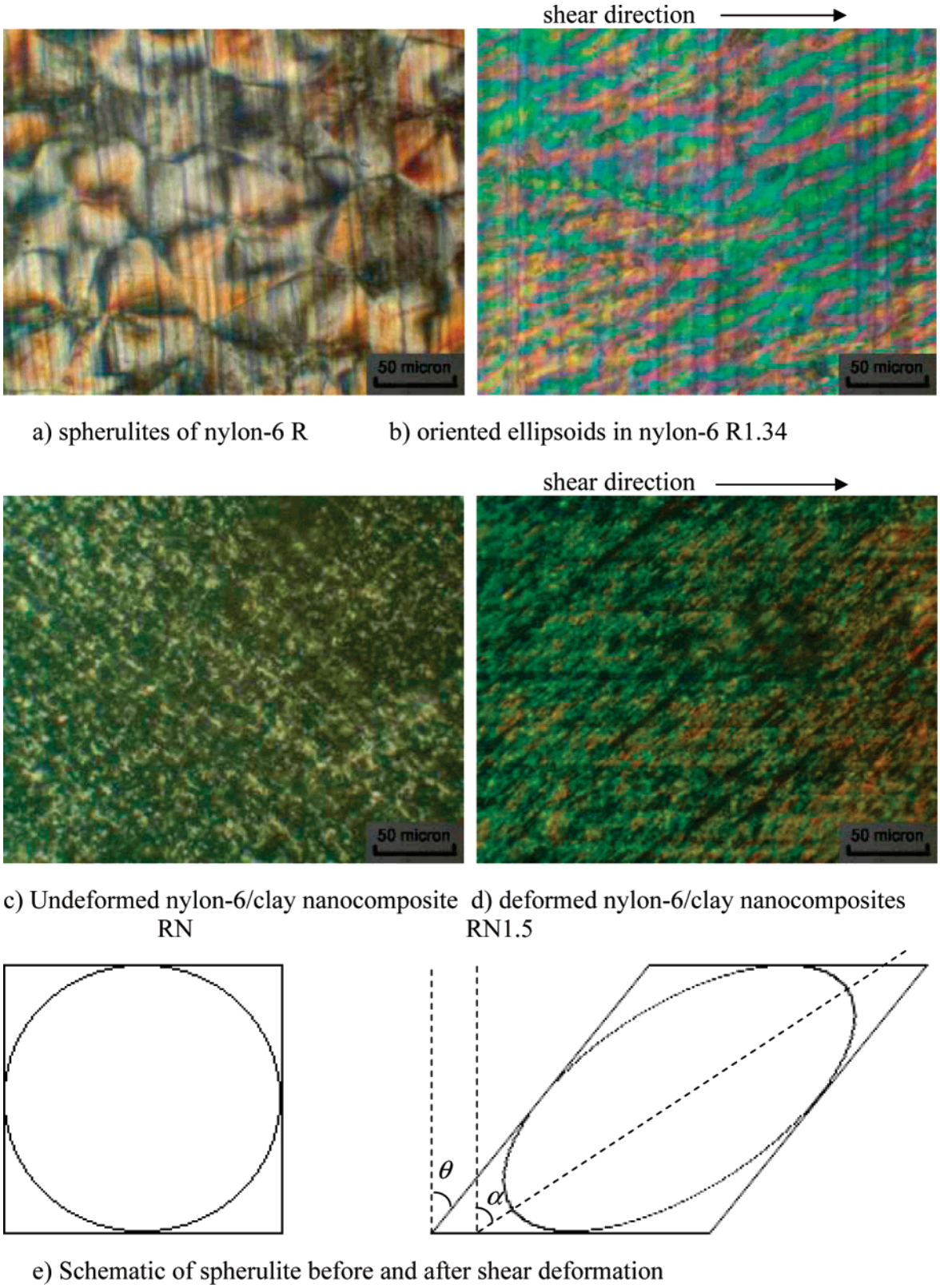

Figure 7. Relationship between shear angle θ and long axis orientation angle α of ellipsoids: (a) spherulites of nylon-6; (b) oriented ellipsoids in nylon-6 R ($\gamma = 1.34$); (c) undeformed nylon-6/clay nanocomposites; (d) deformed nylon-6/clay RN ($\gamma = 1.5$); (e) schematic diagrams of spherulite before and after shear deformation.

in this particular azimuthal direction. More complete details of the deformation-induced orientation appear later in this paper.

In order obtain further information regarding the effects of the ECAE process, polarized light optical microscopy was used to study the deformation of the various materials. Figure 7 shows the optical micrographs of the thin sections from billets of R and RN between crossed polars both before and after the ECAE process. The relatively perfect crystal spherulites of the nylon-6 in Figure 7a have a radius of about 40 μm. After the ECAE process, the spherulites appear as shown in Figure 7b, which are highly elongated into ellipsoids with their long axis rotated clockwise away from the normal direction by an angle that will

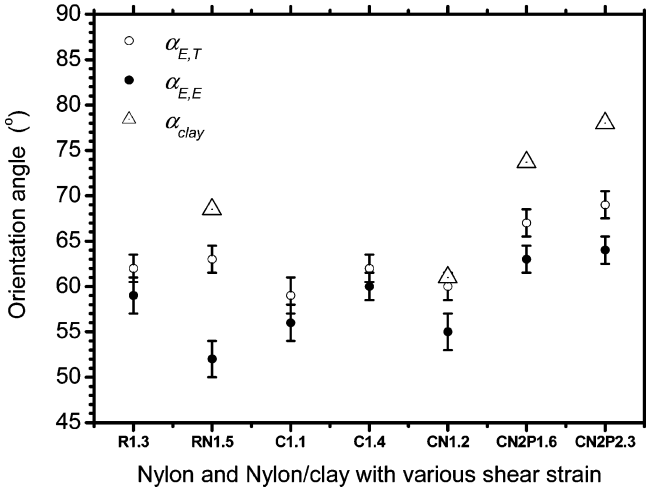

Figure 8. The calculated ellipsoid orientation $\alpha_{E,T}$ from apparent shear strain, the crystal ellipsoid orientation angle $\alpha_{E,E}$ from polarized optical microscope investigation, and the orientation angle of the clay layers α_{clay} produced by ECAE process.

be designated $\alpha_{E,E}$. Figure 7c shows the polarized optical micrograph of RN. The addition of the clay in the RN composite reduces the spherulitic structure to a much finer scale microstructure. This is in good agreement with the reports on nylon-1212/clay[17] and polypropylene/clay nanocomposites.[18] After deformation, although the spherulites have been extremely distorted, the spherulitic morphological structure is also apparently oriented along a specific direction, clockwise from the normal direction by an angle $\alpha_{E,E}$ (from Figure 7d).

If the spherulites are assumed to be deformed by shear in the same way as the overall material (i.e., affinely) and the volume of the spherulite is constant, an initially (assumed spherical) spherulite will transform into an ellipsoid, which would correspond to the principal strain ellipsoid. The theoretical relation of the orientation angle α of the major axis of the ellipsoid and the shear angle θ is given by[2,19]

$$\alpha = \frac{1}{2}\arctan\left(-\frac{2}{\gamma}\right) \tag{2}$$

where

$$\gamma = \tan(\theta) \tag{3}$$

The predictions of α based on this equation, from the measured values of θ, are plotted in Figure 8, designated as $\alpha_{E,T}$. For one pass under similar ECAE conditions, R and RN attain similar apparent plastic shear strain. For the pure nylon-6 (R and C), the values of $\alpha_{E,E} = 59° \pm 2°$, $56° \pm 2°$, and $60° \pm 2°$ observed using polarized optical micrography are quite close to the assessed $\alpha_{E,T} = 62° \pm 1°$, $59° \pm 1°$, and $62° \pm 1°$. This result is in agreement with similar observations reported on poly(ethylene terephthalate) after ECAE deformation.[2] However, for the nylon-6/clay nanocomposites CN and RN, there is a significant discrepancy between the calculated $\alpha_{E,T}$ and the experimental $\alpha_{E,E}$. This seems to indicate that the deformation of the crystallites of the nanocomposite is in some way different from that in pure nylon-6. This could be attributed to the existence of the clay layers (with thickness of about 1 nm and length of about 50−500 nm) in the polymer matrix. If the clay layers are dispersed uniformly in the polymer matrix and supposing the size of each individual clay layer to be $1 \times 200 \times 200$ nm^3, there are approximately 600 clay layers in 1 μm^3 for a 5% clay loading and (say) 250 layers in 1 μm^3 of the 2% clay nanocomposite. Although the polymer spherulites in the nylon/clay nanocomposites are very small, they still have a size of the order 1 μm in diameter, and so it can be deduced that each of them potentially contains some thousands of clay layers. This large number of clay layers has the potential to influence the deformation within a spherulite and possibly cause the spherulite to fragment into fine crystallites, with subsequent nonaffine deformation of the spherulitic microstructure.

To gain understanding of the effect of clay on the deformation of the polymer, the orientation of the clay layers under ECAE process was studied using small angle X-ray scattering (SAXS). The average orientation of the clay layers in the nylon-6/clay nanocomposites was investigated by performing SAXS through the transverse direction of the samples both before and after ECAE.

The SAXS image for original nylon-6 R with the X-ray beam perpendicular to the compression direction of the compression molded sample (shown in Figure 9a) shows a clear uniform scattering from the polymer crystal lamellae. Wide angle X-ray patterns also show a nonoriented ring pattern. This suggests that no significant crystalline orientation occurs during compression molding. A typical SAXS image of nylon-6/clay nanocomposite RN (shown in Figure 9b) obtained with the X-ray beam perpendicular to the compression direction shows much stronger scattering which must be be attributed to the presence of clay. This scattering image does not show evidence of any orientation suggesting that no pre-existing orientation of clay layers is present in the 10 mm thick sample prepared by compression molding. The SAXS of R2P1.81TD shows orientation typical of nylon-6 crystal lamellae. It is difficult to quantify a specific orientation angle of the crystal lamellae because the scattering pattern comprises two asymmetrical arcs, suggesting a broad distribution of lamellar normals centered in a particular direction. This center of the distribution of the normal directions of the oriented crystal lamellae is shown as an arrow in Figure 9c. The nylon-6/clay nanocomposite RN2P1.57TD displays strong scattering anisotropy, indicating that the normals of the clay layers are distributed around the direction shown by the arrow in Figure 9d. The orientation angle of the clay layers can be measured from the strong scattering pattern, and some typical results are plotted in Figure 8 as α_{clay}. It can be seen that α_{clay} is always higher than the actual crystal ellipsoid orientation angle $\alpha_{E,E}$ from polarized optical microscope. Because the orientation of a semicrystalline polymer in a clay-reinforced nanocomposite depends significantly upon the clay orientation,[12] a more advanced clay orientation will induce crystal lamellae orientation and further cause the fragmentation of crystal spherulites and nonaffine deformation of the spherulitic microstructure.

To gain further understanding of the effects of deformation on the morphology of the different polymer compounds under study, samples of the different polymers were subjected to tensile drawing (see ASTM D638) to form a basis for comparison of the structures obtained. Figure 10a displays the WAXD flat plate pattern of a stretched nylon-6 sample R with the beam perpendicular to the horizontal tensile direction. The sample R was highly stretched (extension ratio $\lambda = 2.7$ or a nominal strain of 170%) at room temperature, and the diffraction from the (002) and (200) planes is strongly aggregated on the equatorial plane. This suggests that the *a* and *c* axes are largely normal to that plane although there is no distinct diffraction peak for planes perpendicular to the macromolecular chains (the *b* axis for the α-form crystal of nylon-6), the preferred orientations of the *a* and *c* axes. Both are largely perpendicular to the drawing direction which indicates that the majority of α

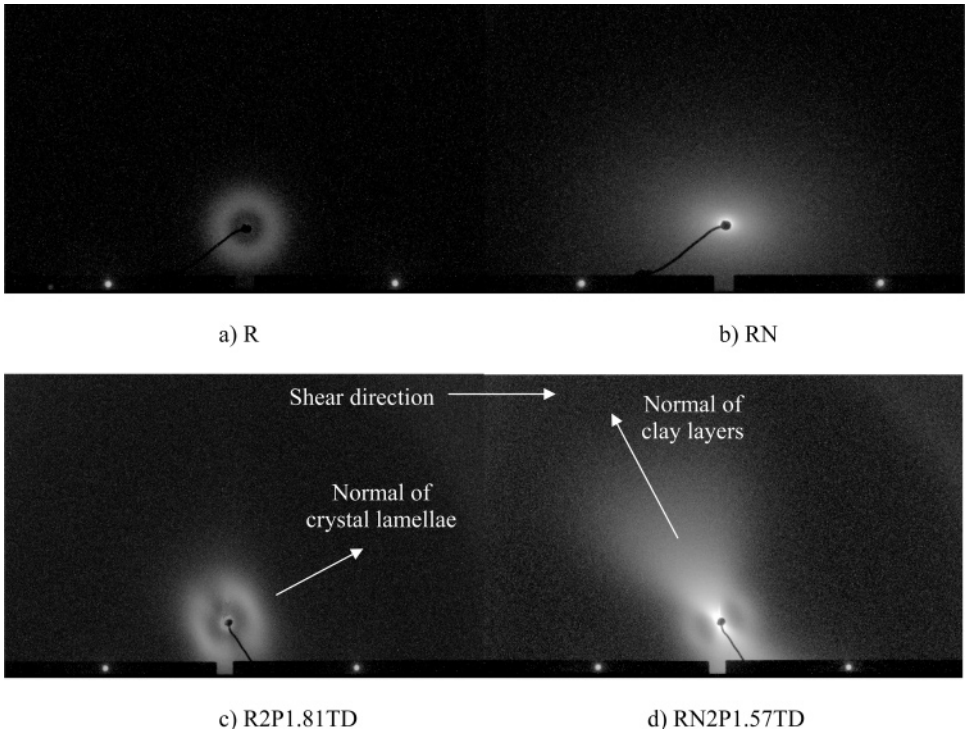

Figure 9. The SAXS images of (a) compression molded nylon-6 R with the X-ray beam perpendicular to the compression direction; (b) compression molded nylon-6/clay RN with the X-ray beam perpendicular to the compression direction; (c) nylon-6 R after two ECAE passes, with a strain of 1.81 and the X-ray beam in the transverse direction; and (d) nylon-6/clay RN after two ECAE passes, with a strain of 1.57 and the X-ray beam in the transverse direction.

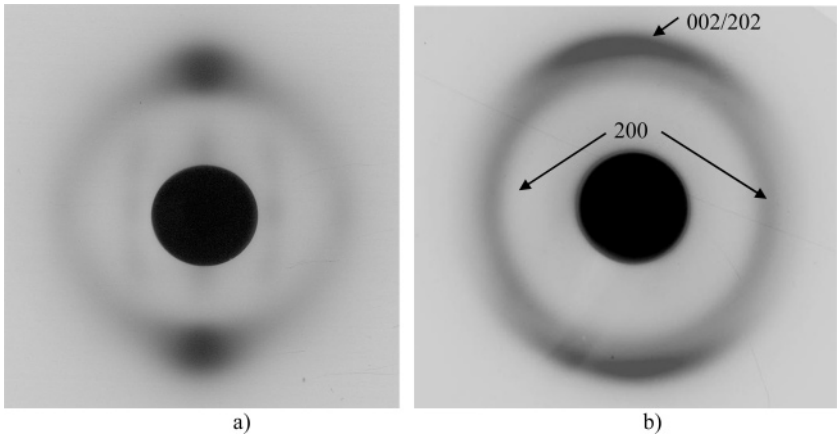

Figure 10. The WAXD flat plate patterns of nylon-6 after (a) tensile stretching along the horizontal direction with extension ratio $\lambda = 2.7$ and (b) channel die compression (CD) along the vertical direction, with tensile strain (FD) along the horizontal direction, shear strain $\gamma = 1.4$, and the X-ray beam along TD.

crystallites are aligned with their *b* axis along the tensile deformation direction, typical of a fiber orientation.

Figure 10b shows the WAXD flat plate pattern of the nylon-6 after pure shear by CDC, where the X-ray beam is directed along the transverse direction TD (see Figure 2). The maximum intensity from the (002) plane is along the compression direction (CD in Figure 2), while the intensity minimum from (200) is also in this direction. On the basis of the interpretation of the chain slip mechanism proposed by Argon,[20−23] the possible orientation of the α-form crystal lattice in nylon-6 is displayed schematically in Figure 11. Generally, the orientation of the molecular chains is along the flow direction (FD), shown in Figure 11 as the *b* axis. The maximum intensity in CD indicates the main orientation of the (002) planes with their normals (designated by c*) along CD. For the monoclinic unit cell of α nylon-6 crystals, the normal of the (200) plane (a*) is distributed about a direction that is 67.5° (angle β, shown in Figure 11) away from TD. The characteristic diffraction patterns from nylon-6/clay nanocomposites show a similar orientation of the (002) and (200) planes, suggesting a similar trend in the orientation of α crystallites in both nylon-6 and nylon-6/clay nanocomposites after the pure shear.

The intensity changes after ECAE deformation of the characteristic diffraction peaks in the three directions of neat nylon-6 samples (R, C) and nylon-6/clay nanocomposites (RN, CN) are displayed in the WAXD flat film patterns in Figure 12. The normal to each respective face of the cube as shown on the set of axes is the direction of the X-ray beam used to obtain the diffraction image displayed on that face. Compared with the diffraction from undeformed samples, the intensity of the (200) and (002) peaks changed after the ECAE process, indicating preferred orientation of the crystal planes.

With the X-ray beam directed along the normal direction (ND in Figure 12), the (002) diffraction peak is the same as those of

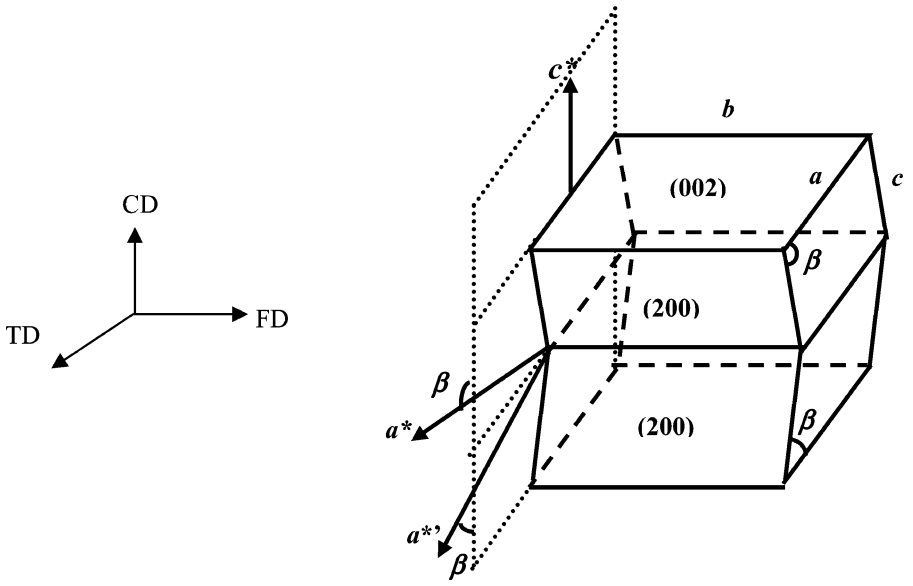

Figure 11. Schematic diagram of the main orientation of the crystal planes.

the undeformed samples. The (200) intensity increases along a spread of azimuthal angle around the transverse direction (TD), indicating that the normal of the (200) planes is probably orientated along TD. The pattern also displays mirror symmetry with respect to both the SD and the TD. If the X-ray beam is directed along SD, the (200) diffraction increases in intensity around TD, which is in agreement with the information from ND. The intensity from the (002) planes increases around ND, which suggests that some of the (002) plane normals are oriented along ND. The diffraction images from the SD directed beam also display mirror symmetry with respect to the transverse and normal directions.

The most informative diffraction evidence about orientation appears on the TD diffraction images. With an increase in shear strain, the (002) diffraction intensity aggregates as a set of azimuthal arcs for a specific direction while the azimuthal minima of the (200) diffraction are also in this direction. The bimodal orientation, which is commonly found in deformed HDPE and PP,[1] is not apparent for the α crystalline form of nylon-6 and nylon-6/clay nanocomposites after the ECAE process.

It can be seen that all the diffraction images from illumination along ND, SD, and TD display maximum and minimum diffraction directions that indicate the orientation of the macromolecular crystals. Therefore, a comparison of the diffraction along these directions is potentially a very useful tool to investigate the structural orientation quantitatively. By use of a conventional diffractometer, a measure of the extent of orientation can thus be obtained by orienting the specimen to measure the diffracted intensity along the chosen azimuthal directions. Figure 13 shows typical WAXD curves along the maxima and minima of α (200) and α (002) diffraction for nylon-6 C.

Figure 13b displays the diffraction intensity curves from illumination along the ND of deformed nylon-6 C along the orthogonal directions SD and TD (Figure 13a) compared with a trace taken from an undeformed sample. The intensity has no significant change along SD, while the intensity of (200) increases and that of (002) decreases along TD. It suggests that the chain slip of the (002) planes causes rotation of crystalline lamellae. As a consequence, the c* normals of the (002) planes rotate away from TD and the a* normals of the (200) planes congregate around TD. Given the general tendency of chains to align with SD, the possible orientations of the crystal lattice are schematically shown as A and B in Figure 13a. With the chain direction (*b* axis) along the shear direction, the (002) plane is parallel to the *b* axis and extends to the inside and outside of the plane of the paper. The possible direction of the *a* axis is also displayed in the two possible orientations. Both of them show the normal of (200) parallel to or close to TD by a small angle (about 22.5°, $90 - \beta$) and the normal of (002) away from TD by a relatively large angle (90° or β) so that the oriented crystalline structure causes an increase of the diffraction from the (200) plane and a decrease of the diffraction from the (002) along TD.

Figure 13d displays typical diffraction intensity curves from illumination along SD. There is increased intensity along TD for the (200) reflection and along ND for the (002) peak. The possible orientations of the crystalline lattice are displayed as A and B in Figure 13c. In the A condition, the normal of (002) is parallel to ND and the normal of (200) plane is around TD by a small acute angle (about 22.5°, $90 - \beta$). Under the B condition, the normal of the (002) plane is distributed around ND within a small angle (about 22.5°, $90 - \beta$) and the normal of the (200) plane is parallel to ND.

Figure 13f shows typical diffraction intensity curves from illumination along TD. If the *b* axis is aligned generally along SD, there is only one possible orientation of the (002) plane, i.e., with its normal perpendicular to the diffraction arc shown as A in Figure 13e. The two possible directions of the *c* axis extend to the inside of the plane of the page. The normal of the (200) planes deviates from the TD plane by an angle β, which does not lead to the decrease of the intensity of the (200) in the D_{max} direction. This indicates that the direction of the *b* axis is not precisely aligned along the SD at this stage of deformation but close to the SD by a specific angle, which tends to zero with the increase of shear strain. The main chain orientation direction (MCOD) is orthogonal to the D_{max} of the (002) plane from the TD view. It is clear that the A condition in Figure 13a from ND and the A condition in Figure 13c from SD are in agreement with the result from TD and so the other possibilities are excluded. Therefore, a three-dimensional schematic representation of the possible orientation of the crystalline lattice is as shown in Figure 14. The MCOD is close to SD by a specific angle, and the normal of the (002) plane is mainly oriented along

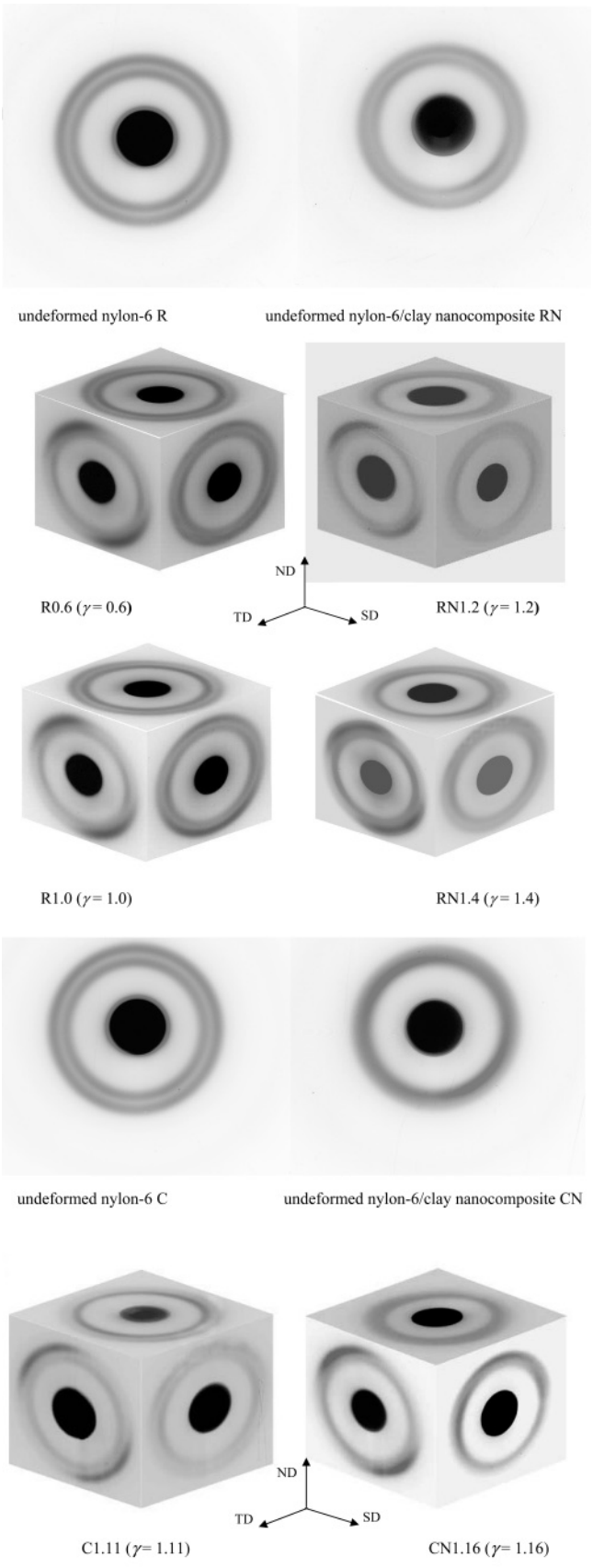

Figure 12. The flat plate film patterns of nylon-6 and nylon-6/clay nanocomposites with various indicated shear strains after the ECAE process.

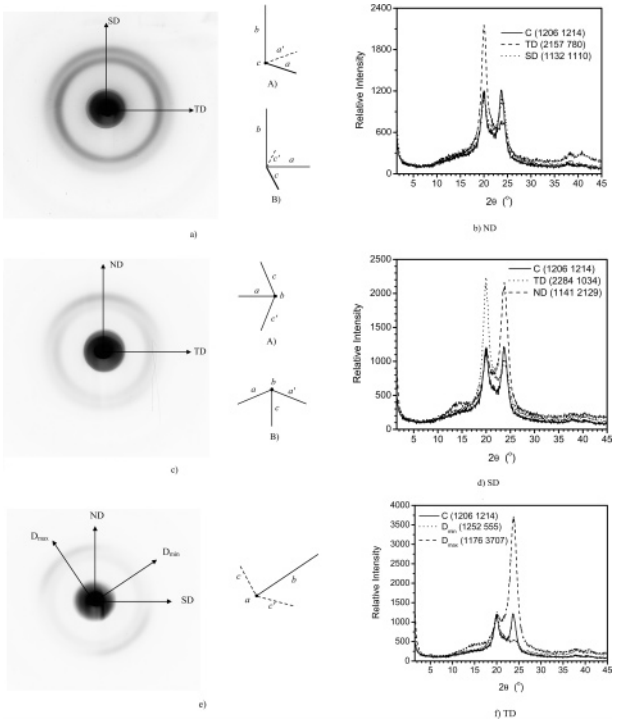

Figure 13. Panels a, c, and e show WAXD flat plate images for nylon-6 C deformed at $T = 150$ °C to a shear strain $\gamma = 1.11$, with the beam along ND, SD, and TD in turn. Also, the possible dominant orientations of the crystalline axes are illustrated. Panels b, d, and f show the WAXD diffractometer traces taken along the radial directions, as indicated in the preceding part of the figure, compared with the diffractometer trace (labeled C) for an undeformed sample of the same material.

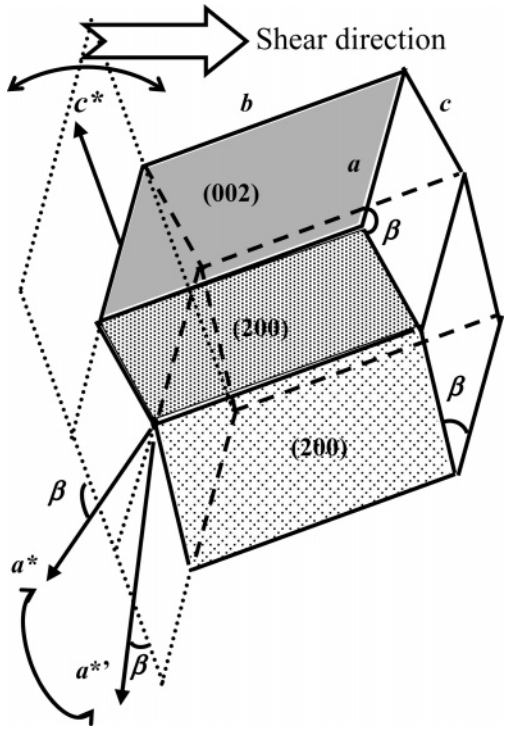

Figure 14. Schematic diagram of the main orientation of the crystal planes.

the MCOD and has a distribution around the MCOD for the tilt of the normal around the MCOD. The two possible normals of (200) planes are distributed around the direction at an angle from TD, and their diffraction folds together for the tilt of the (200) planes to form a set of long azimuthal arcs.

From the diffraction patterns of TD, it is apparent that the orientated crystalline structure resulting from the ECAE process is similar to that obtained by CDC pure shear but the structure

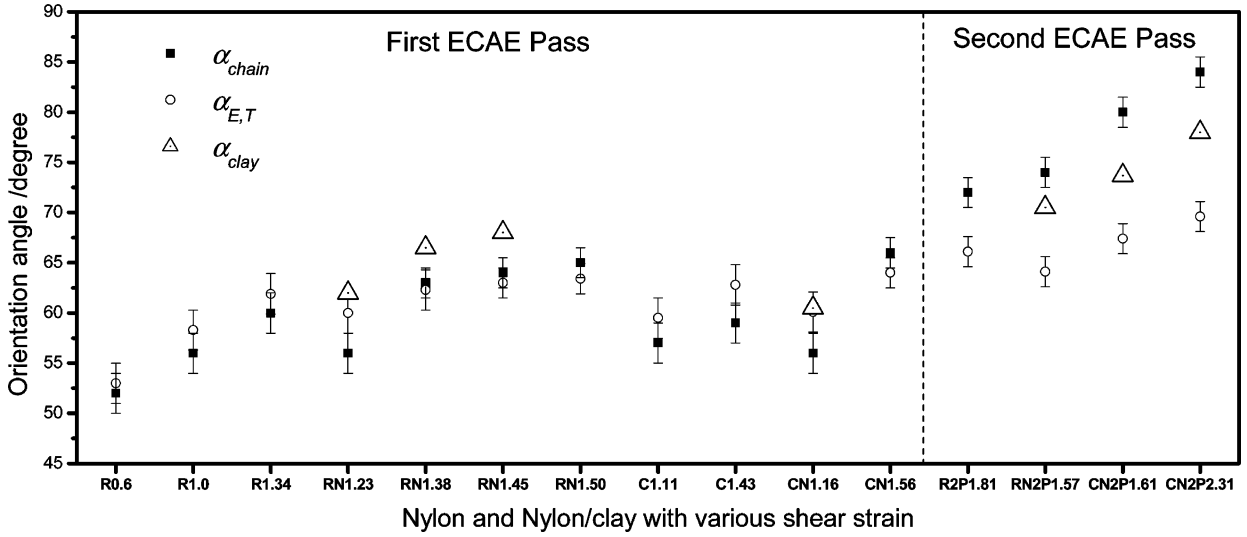

Figure 15. The macromolecular chain orientation angles α_{chain} and calculated spherulite ellipsoid orientation angle $\alpha_{E,T}$ of nylon-6 and nylon-6/clay nanocomposites resulting from ECAE deformation (the numbers followed by the polymer symbols are their apparent shear strain γ). α_{clay} values for the nanocomposites are also shown.

obtained by tensile deformation is somewhat different. The schematic diagram of the main orientation of the crystal lattice from the ECAE process can be obtained by rotating the schematic diagram of the oriented crystal lattice from CDC samples (Figure 11). That the tensile test is different is not surprising, as the tensile test involves a significantly larger strain and a different stress state when compared to samples with one or two passes of ECAE or CDC (unless taken to extremes) and the tensile orientation was done at room temperature whereas the ECAE and CDC were done at elevated temperatures.

The characteristic arcs from (002) diffraction indicate that the simple shear process, due to chain slip along the planes of hydrogen bonds, causes rotation of fragments of lamellae that tend to orient with their (002) planes along the orientation direction of maximum tensile strain. This kind of alignment of the α crystals resembles a twinned monocrystal along the crystallographic planes containing hydrogen bonds,[21] the (002) planes becoming perpendicular to the short axis direction (equivalent to the compression direction in pure shear), with the macromolecular chains aligned along the long axis.[22] The apparent twinning symmetry plane is the (002) plane. It is reasonable to suppose that the main orientation of the crystalline planes after the ECAE process is as shown schematically in Figure 14. With the chains orientated along a direction with a specific angle clockwise away from the normal direction, the normal (c*) of the (002) plane is around the perpendicular line of the chains. Therefore, the diffraction of the (002) plane forms the two arcs with the aggregated intensity on the TD pattern. The normals of the two possible orientations of (002) planes are inclined and folded together to form the diffraction distributed along azimuthal angles around the transverse direction. It can be seen that the azimuthal angular spread of (200) diffraction is bigger than that of the (002) diffraction.

The mean azimuthal orientation angle of the α (002) diffraction, designated as α_{chain}, is a parameter which can be used to describe the extent of orientation of the macromolecular chains in the crystalline phase. The α_{chain} values of nylon-6 and nylon-6/clay nanocomposites after the ECAE process are plotted in Figure 15. The α_{chain} values of the two nylon-6 R and C samples are very close to the theoretically calculated ellipsoid orientation angle $\alpha_{E,T}$, which is in good agreement with orientation of the strain ellipsoid considering the orientation of molecular chain along the long axes of the crystal ellipsoid. Figure 15 also shows the α_{chain} values of the two nylon-6/clay nanocomposites RN and CN being close to their $\alpha_{E,T}$ values and always being associated with the orientation angle of clay α_{clay} from SAXS after the first ECAE process. The α_{chain} is always slightly smaller than the α_{clay} which suggests that the orientation of clay layers has induced the chain orientation. Since the crystal ellipsoids in nylon-6/clay nanocomposites experience nonaffine deformation after ECAE and the orientation of the ellipsoid lags behind the theoretical calculated $\alpha_{E,T}$, the orientation of the molecular chains is not parallel to the long axes of crystal ellipsoids. This also is attributed to the influence of clay layers, and the mechanism is expatiated in detail in the further discussion.

Another interesting result is that, after a second ECAE pass, the nylon-6/clay nanocomposites obtain a relatively high apparent strain and high chain orientation with the α_{chain} values significantly enhanced to more than 80°, which is very close to the shear direction (90°). It could be surmised that after enough ECAE passes, the crystalline molecular chain axis would fully align with the shear direction. Although RN1.57 has lower shear strain than R1.81, its α_{chain} is much higher than that of R1.81. Furthermore, the in situ polymerized CN obtained the highest α_{chain} due to the primary chemical bonds between clay and molecular chains. These observations strongly support the clay-induced chain orientation mechanism.

From the above discussion, a deformation mechanism is summarized as shown schematically in Figure 16. When the α form of crystal is dominant, the orientation of the molecular chains is associated with the orientation of the crystal lamella as shown in Figure 16a. The MCOD is orthogonal to the orientation direction of crystal lamella shown in Figure 9. The orientation of crystal lamellae is governed by the affine deformation of the crystal ellipsoid during the first ECAE process. For the nylon-6/clay nanocomposites shown in Figure 16b, the clay layers play an active role in inducing the orientation of the molecular chains and the crystal lamellae. Due to the slip and rotation of the clay layers, the macromolecular chains are induced to slip evenly and continuously throughout the crystal lamellae and lend to the rotation and orientation of crystal lamella. Because of the realignment, the orientation of crystal lamellae lags behind that of the macromolecular chains, which is almost oriented along the direction of clay layers. This also contributes to the nonaffine deformation of the spherulites.

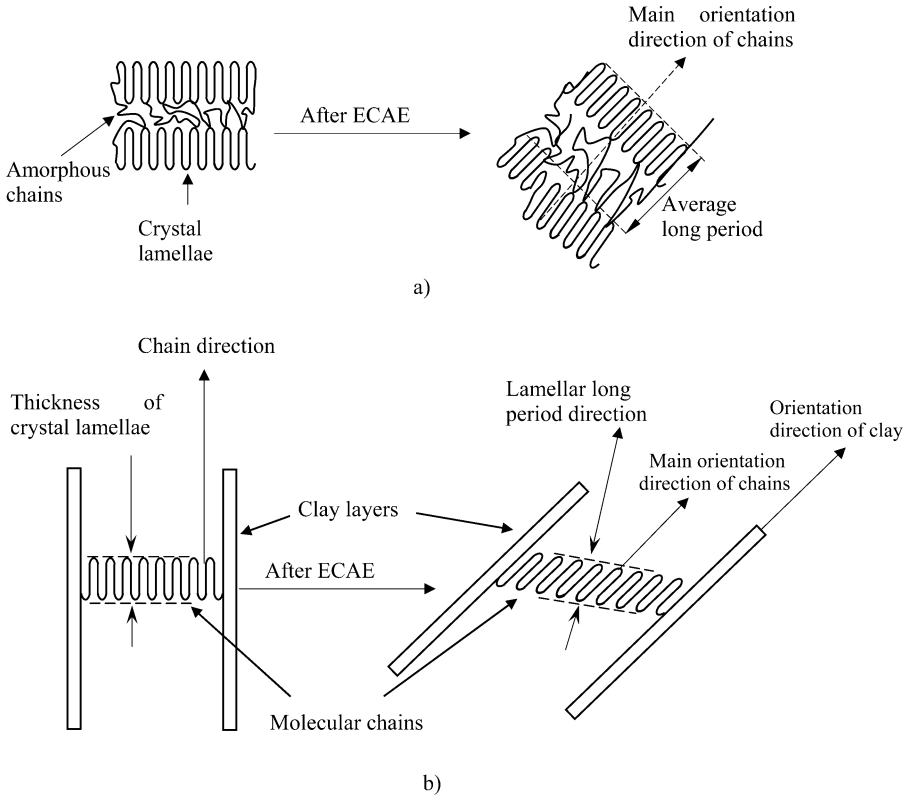

Figure 16. The schematic diagrams of clay layer slip and rotation mechanism during ECAE process: (a) nylon-6; (b) nylon-6/clay nanocomposite (chain orientation induced by clay layers).

When further deformed in the second ECAE process, the slip of the clay layers will stretch the molecular chains and the crystal lamellae in between to induce even higher orientations of the molecular chains. As shown in Figure 15, the molecular chains of nylon/clay nanocomposites achieved higher orientation than the clay layers. The well dispersed clay layers and their tight connection with molecular chains in the in situ polymerized nanocomposites (compared to melt blended materials)[24−25] clearly improve the nanoclay influence, and CN shows the highest α_{chain}. This mechanism can explain why nylon-6/clay nanocomposites deform with less stress on the second ECAE pass and also why synthesized CN obtains the highest shear strain with the lowest stress as shown in Table 1. At the first ECAE pass, due the random orientation and location of the clay, it is very difficult to deform the composite material, so a higher stress is needed (see Table 1). After the first ECAE process, some of the clay platelets will be oriented with their planes along either the shear direction or the major strain axis, making the nylon-6/clay nanocomposite more easily deformed. The tighter chemical bond in CN between clay layers and the macromolecular chains from in situ intercalative polymerization[24,25] possibly make the effects of the clay on shear deformation more significant than that in the melt compounded RN. The orientation of clay layers dominates the morphology of the nanocomposites by inducing the orientation of molecular chains and crystal lamellae. This orientation behavior is a further dominating factor for mechanical property improvements of these polymer nanocomposites.[13]

Conclusions

Nylon-6 and nylon-6/clay nanocomposites, formed either by in situ polymerization or by melt blending with similar contents of nanoclay, were deformed in the solid state by the equal channel angular extrusion process, and the morphology of the resultant materials were determined by a range of techniques. In order to obtain a high permanent shear strain by the 90° ECAE process, it was found that an optimum deformation temperature of about 150 °C for both nylon-6 and nylon-6/clay nanocomposites was required. Nylon-6 experienced affine deformation during a ECAE process while the nylon-6/clay nanocomposites produced nonaffine deformation on comparison of the calculated orientation angle of ellipsoids $\alpha_{E,T}$ based on the principle of the affine deformed ellipsoids. A schematic representation of the effect of ECAE deformation on the primary orientation of the crystal lattice of the α crystal was suggested based on the analysis of the diffraction of the α (002) and α (200) planes in three dimensions. The chain slip of the hydrogen-bond-containing (002) plane in the α crystalline form was the active mechanism of the orientation of the macromolecular chains of nylon-6 during the ECAE process. The change in orientation of the clay layers during the ECAE process caused the nylon-6/clay nanocomposites to achieve high shear strain. The clay layer slip mechanism showed that the shear force during the ECAE process leads to the slip and rotation of the clay layers in the crystalline region, which induced the even and continuous molecular chain slip. The slip and rotation of clay layers caused a nonaffine deformation of the crystal ellipsoids in nylon/clay nanocomposites, leading to the high orientation of the macromolecular chains for any subsequent ECAE passes. The in situ polymerized nylon-6/clay nanocomposites achieved the highest molecular chain orientation due to the chemical bonds between clay layers and molecular chains.

References and Notes

(1) Campbell, B.; Edward, G. H. *Plast. Rubber Compos.* **1999**, *28*, 467−475.
(2) Xia, Z. Y.; Sue, H. J.; Rieker, T. P. *Macromolecules* **2000**, *33*, 8746−8755.
(3) Sue, H-J.; Dilan, H.; Li, C. K-Y. *Polym. Eng. Sci.* **1999**, *39*, 2505−2515.
(4) Ward, I. M. *Adv. Polym. Sci.* **1985**, *70*, 1−70.

(5) Xia, Z.; Sue, H. J; Hsieh, A. J. *J. Appl. Polym. Sci*. **2001**, *79*, 2060−2066.
(6) Li, C. K-Y.; Xia, Z-Y.; Sue, H-J. *Polymer* **2000**, *41*, 6285−6293.
(7) Coulon, G.; Castelein, G.; G'sell, C. *Polymer* **1998**, *40*, 95−111.
(8) Usuki, A.; Kojima, Y.; Kawasumi, M.; Okada, A.; Fukushima, Y.; Kurauchi, T.; Kamigaito, O. *J. Mater. Res.* **1993**, *8*, 1179−1183.
(9) Mathias, L. J.; Davis, R. D.; Jarrett, W. L. *Macromolecules* **1999**, *32*, 7958−7960.
(10) Liu, L.; Qi, Z.; Zhu, X. J. *Appl. Polym. Sci.* **1999**, *71*, 1133−1138.
(11) Nair, S. Smitha; Ramesh, C. *Macromolecules* **2005**, *38*, 454−462.
(12) Weon, J.-I.; Xia, Z.-Y.; Sue, H.-J. *J. Polym. Sci., Part B: Polym. Phys.* **2005**, *43*, 3555−3566.
(13) Weon, J.-I.; Sue, H.-J. *Polymer* **2005**, *46*, 6325−6334.
(14) Tung, J.; Gupta, R. K.; Simon, G. P.; Edward, G. H. *Weld lines behaviour in melt blended and in situ polymerised nylon-6 nanocomposites*, ANTEC 2004 Conference Proceedings, Chicago, Illinois, May 16−20, 2004; Society of Plastics Engineers: Brookfield, Connecticut, 2004; Vol. 1.
(15) Li, Youyong; Goddard, A. W. *Macromolecules* **2002**, *35*, 8440−8448.
(16) VanderHart, D. L.; Asano, A.; Gilman, J. W. *Chem. Mater*. **2001**, *13*, 3796−3809.
(17) Wu, Z.; Zhou, C.; Zhu, N. *Polym. Test.* **2002**, *21*, 479−483.
(18) Ma, J.; Zhang, S.; Qi, Z.; Li, G.; Hu, Y. *J. Appl. Polym. Sci.* **2002**, *83*, 1978−1985.
(19) Nadai, A. In *Theory of Flow and Fracture of Solids;* McGraw-Hill: New York, 1950; Vol. 1, Part 1, p 147.
(20) Galeski, A.; Argon, S.; Cohen, R. E. *Macromolecules* **1991**, *24*, 3953−3961.
(21) Lin, L.; Argon, S. *Macromolecules* **1992**, *25*, 4011−4024.
(22) Galeski, A.; Argon, S.; Cohen, R. E. *Macromolecules* **1988**, *21*, 2761−2770.
(23) Galeski, A.; Argon, S.; Cohen, R. E. *Macromolecules* **1991**, *24*, 3945−3952.
(24) Ma, J.; Qi, Z.; Hu, Y. *J. Appl. Polym. Sci.* **2001**, *82*, 3611−3617.
(25) Okada, A.; Usuki, A. *Macromol. Mater. Eng.* **2006**, *291*, 1449−1476.

MA071580O